OVER-THE-WING-NACELLE-MOUNT CONFIGURATION FOR NOISE REDUCTION

Daisuke Sasaki*, Ryota Yoneta*, Kazuhiro Nakahashi*
***Department of Aerospace Engineering, Tohoku University**

Keywords: *aircraft design, over-the-wing-nacellel-mount configuration*

Abstract

An Over-the-Wing-Nacelle-Mount airplane configuration is known to prevent the noise propagation from jet engines toward ground. However, the configuration is assumed to have low aerodynamic efficiency due to the aerodynamic interference effect between a wing and a nacelle. In this study, aerodynamic design optimisation is conducted to improve aerodynamic efficiency to be equivalent to conventional Under-the-Wing-Nacelle-Mount configuration. The nacelle and wing geometry are modified to achieve high lift-to-drag ratio, and the optimal geometry is compared with conventional configuration. Pylon shape is also modified to reduce aerodynamic interference effect. The final geometry is compared with conventional geometry of DLR F6 model to discuss the potential of OWN geometry for an environmental-friendly future aircraft.

1 Introduction

With the growth in aircraft traffic, there is a strong demand to reduce the airport noise. The major sources of the airport noise are jet and fan noises caused by the engine. In all over the world, regulations on airport noise have been tightened, thus it is a significant problem to reduce airframe and engine noises.

One of the potential solutions to reduce the engine noise is to adopt an Over-the-Wing-Nacelle (OWN) configuration which can block the propagation of fan and jet noises toward ground [1]. However, the configuration tends to lead low aerodynamic performance due to the interference effect between a wing and a nacelle.

Therefore, the purpose of this study is to investigate the aerodynamic feasibility of OWN configuration by making use of Computational Fluid Dynamics (CFD) and optimisation methods. The cruise Mach number is set to 0.70 to focus on mid-sized, short-range aircraft for the domestic use. In this study, aerodynamic interference effect between a nacelle and a wing is optimised through the modification of nacelle, wing and pylon shapes.

2 Optimisation System

2.1 Flow Analysis

In this research, wing-fuselage configuration with a nacelle and a pylon is analysed using three-dimensional unstructured mesh CFD solver, TAS (Tohoku University Aerodynamic Simulation) code [2, 3]. The compressible Euler equations are solved by a finite-volume cell-vertex scheme. The numerical flux normal to the control volume boundary is computed using an approximate Riemann solver of Harten-Lax-van Leer-Einfeldt-Wada (HLLEW) [4]. The second-order spatial accuracy is realised by a linear reconstruction of the primitive gas dynamic variables inside the control volume with Venkatakrishnan's limiter [5]. The LU-SGS implicit method for unstructured meshes [6] is used for the time integration. Accuracy of the TAS-Code has been validated for various flow problems [2, 3].

2.2 Optimisation Method

In aerodynamic shape optimisations, non-linearity of the objective functions must be taken into consideration. Therefore, an in-house

solver of real-coded GA is adopted [7]. It is a population-based optimisation method simulating the evolutionary process of creatures, in which the population evolves over generations to minimise/maximise the objective functions with the operations of selection, crossover and mutation. It is well-known that GA requires large computational cost due to population-based search, particularly coupled with expensive CFD solvers. Therefore, the Kriging model [8, 9] is adopted to build an approximation model of the objective functions to reduce the computational burden. Optimal solutions are searched over the approximation model by Multi-Objective GA [7]. The flowchart of the current optimisation system is shown in Fig. 1. The first sampling points are determined by the Latin Hypercube sampling method [10] to distribute the points in equi-distance space. Kriging approximation model is then constructed based on the sample data, and the model is used for the objective function evaluation in the optimisation process. In this study, the objective function is transformed to the corresponding Expected Improvement (EI) to find the global optimal point robustly

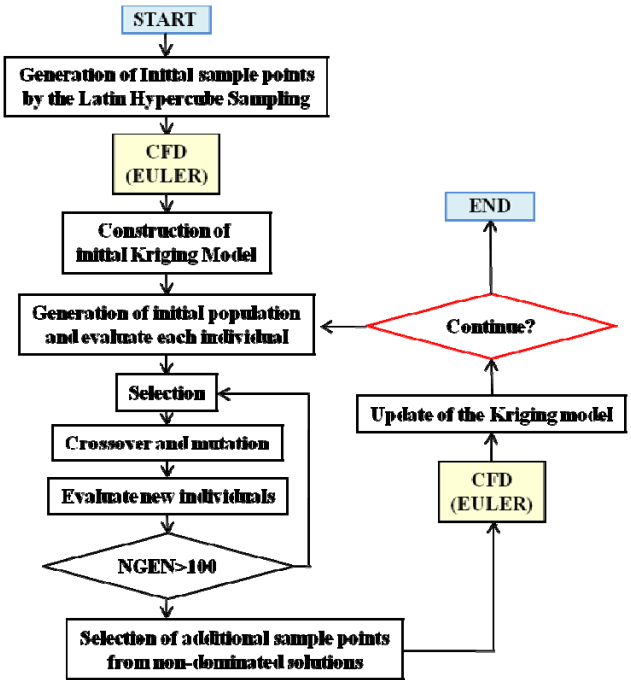

Fig. 1 Flowchart of Aerodynamic Design System

3 Wing and Nacelle Optimisation

3.1 Overview

Wing-fuselage-nacelle-pylon configuration is considered to be an analysed geometry. In this section, nacelle and wing shapes are modified to improve aerodynamic performance by reducing the aerodynamic interference effect between a wing and a nacelle.

3.2 Problem Definition

3.2.1 Objectives and Constraint

The aim is to investigate the feasibility of aerodynamically-efficient OWN configuration with consideration of structural and maintenance necessities. For this purpose, geometric parameters of nacelle location are chosen to be optimised as an incentive to more realistic design.

Objectives:

1. Maximise Cruise L/D
2. Minimise Nacelle Height (Z/c)
3. Minimise Nacelle Rearward Location (X/c)

Constraints:

1. constant C_L =0.57

Number of design variables: 44

Here, in addition to improve aerodynamic efficiency by maximising L/D, minimisation of X/c and Z/h are introduced for preferred geomety. This enables to find high L/D configuration with a nacelle located rearward and lower height.

3.2.2 Geometry Definition

In this section, the nacelle position and shape are optimised, while the pylon shape is fixed to NASA SC(2)-0008 airfoil. Horizontal and vertical tails are not modelled as it does not affect the whole aerodynamic performance.

The nacelle position is defined by two design variables (X/c, Z/h) representing front-rear and vertical movement. The lower surface of nacelle is defined by Bezier surface of four by four control points shown in Fig. 2. Bezier surface is controlled by the x, y, z coordinates of intermediate four control points, which correspond to 12 design variables

(4×3=12variables). The upper surface of nacelle is frozen to original DLR-F6 type [11].

In addition to the nacelle shape and position, the wing shape is also modified for the further improvement in L/D. The 3-D wing shape is defined by the following 30 design variables to control the airfoil shapes. The root, tip and kink sectional airfoils are defined by nine design variables each according to the PARSEC definition [10, 12] as shown in Fig.3. The remaining sectional airfoils are linearly interpolated. In such parameterisation, the complex shape of each airfoil can be represented by a relatively small number of meaningful engineering parameters such as the crest of the upper surface's Z coordinate (Z_{up}), the crest of the lower surface's Z coordinate (Z_{lo}) and the leading edge radius (r_{LE}). This engineering parameterisation is useful for designers to analyze optimised data directly. In addition, the wash-out is defined by two design variables at tip and kink position (T_{kink}, T_{tip}). Furthermore, the incidence angle (θ) is defined at root position. In this optimisation, the planform of the wing is frozen to original DLR-F6 type. The planform with the design (kink) section is shown in Fig. 4.

There are 44 design variables in total. When a new geometry is defined, firstly the designed lower nacelle surface is combined with the upper surface of DLR-F6's nacelle, the new surface mesh is then generated based on the advancing front method [13]. The tetrahedral volume mesh is finally generated using Delaunay approach [14]. Qualitative volume mesh for a new wing-fuselage-pylon-nacelle configuration is always generated with the number of nodes around 1.3 million.

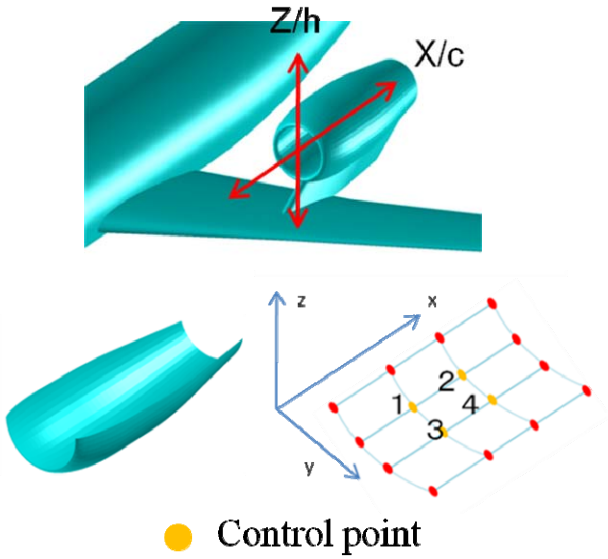

Fig. 2 Nacelle Position and Shape Defintion

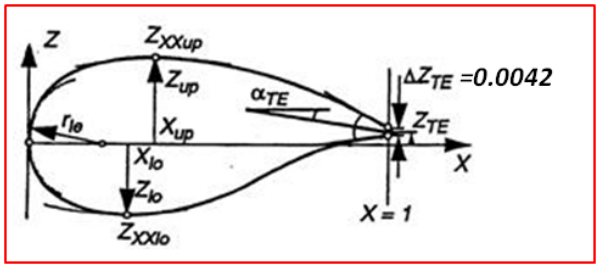

Fig. 3 PARSEC Airfoil Definition

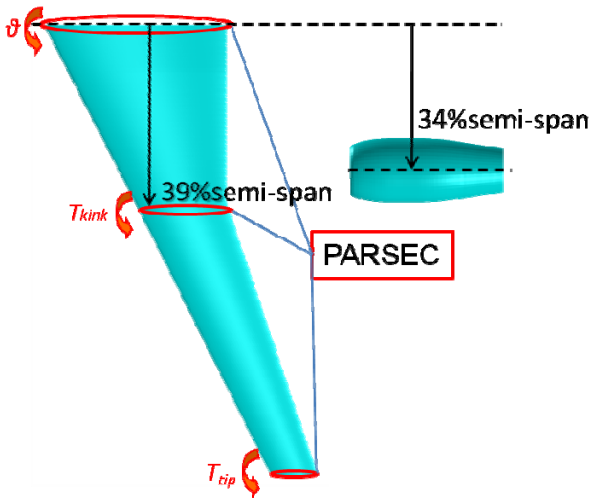

Fig. 4 Planform Shape and Nacelle Location

3.3 Optimisation Results

The first Kriging model was constructed using 79 sample points of the Latin Hypercube sampling. The cross validation of this model is shown in Fig. 5, and it indicates that a reasonable approximation model was constructed. The final Kriging model was

constructed with 169 sample points in total after 12 updates. Several non-dominated solutions on the approximate model were chosen at each update to increase accuracy of the approximation.

Figure 6 shows objective-function space, which means the relation between L/D and nacelle position parameters. Due to the introduction of sub-objectives (X/c and Z/h), optimiser found higher L/D configurations at the nacelle position forward (low X/c) and lower height (low Z/h). One configuration having low X/c and Z/h parameters is chosen from non-dominated solutions (*OPT1*), whose nacelle position parameters are X/c of 0.73 and Z/h of 0.48. This configuration achieved L/D of 34.5 at adjusted angle of attack of 5.71 degrees.

Mach number distributions of *ORIGINAL* (L/D of 25.0) and *OPT1* geometries at 32 % and 37% semi span locations (viewed in Fig. 7) are shown in Figs 8 and 9 respectively. From these figures, the shock wave of the *OPT1* is much weaker than that of the *ORIGINAL* because the flow channel between a wing and a nacelle is optimised to reduce interference effect. This is mainly due to the modification of lower nacelle shape.

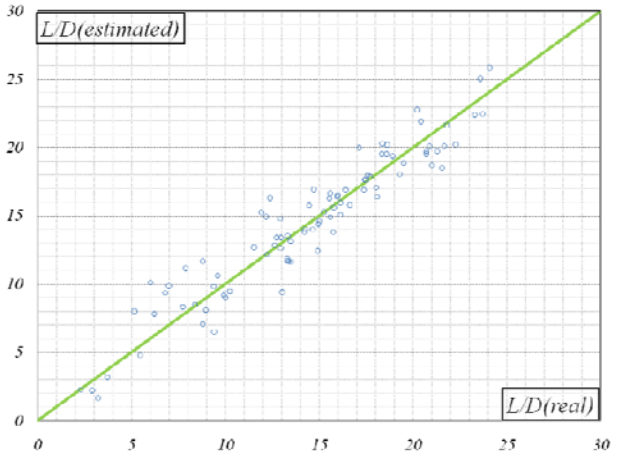

Fig. 5 Cross Validation Result of Kriging Model Built by First Sampling Points

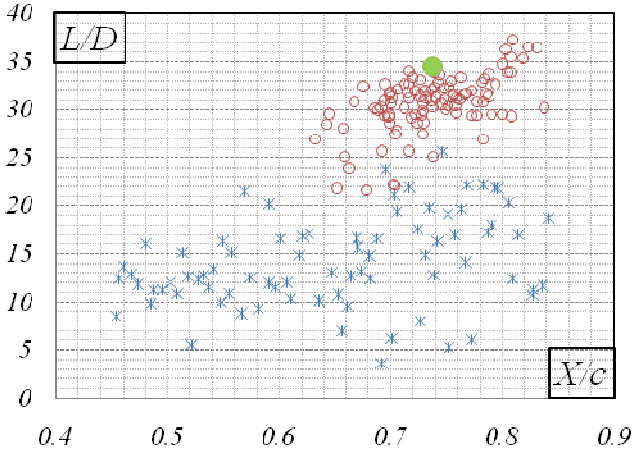

(a) Vertical Movement (X/c)

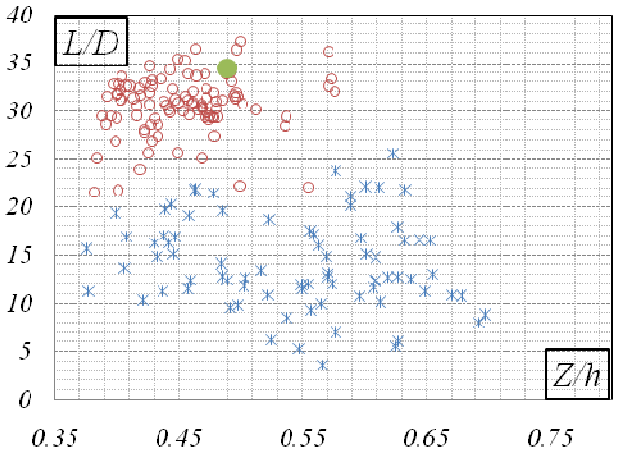

(b) Horizontal Movement (Z/h)

Fig. 6 L/D Distribution against Nacelle Position (blue: initial samples, red: update points)

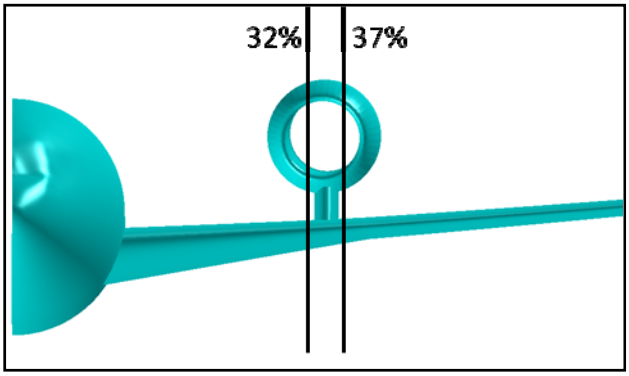

Fig. 7 Cut Planes at Inner and Outer Nacelle

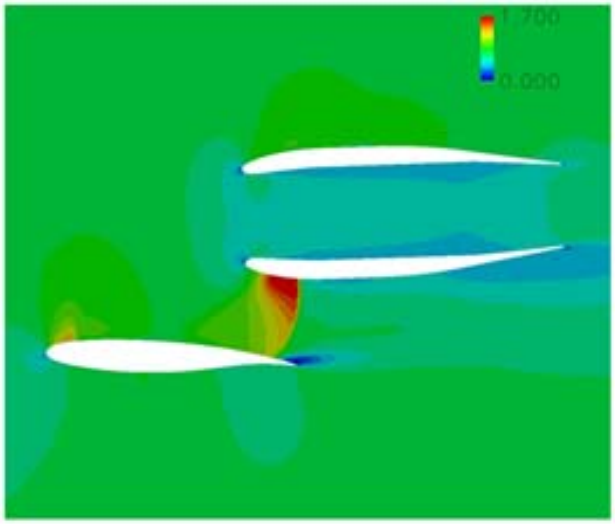

(a) 32% Semi-span Position

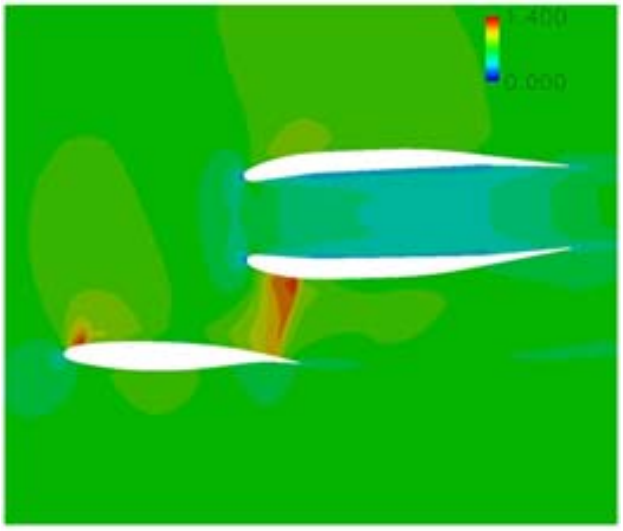

(b) 37% Semi-span Position

Fig. 8 Cp Distribution of *ORIGINAL* Geometry

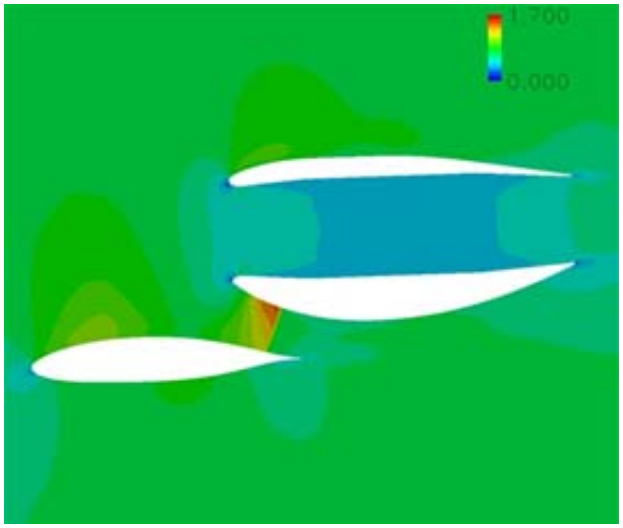

(a) 32% Semi-span Position

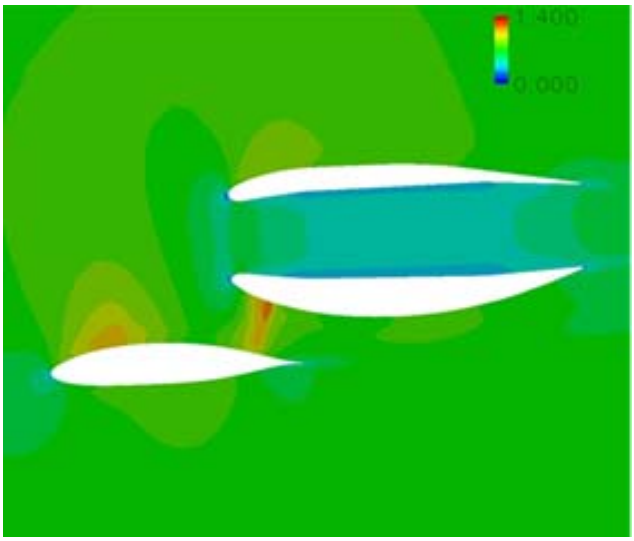

(b) 37% Semi-span Position

Fig. 9 Cp Distribution of *OPT1* Geometry

4 Pylon Optimisation

4.1 Overview

In the previous section, wing and nacelle shapes are modified to improve aerodynamic efficiency. Here, further reduction of interference effect between a wing and a nacelle is intended by optimising a pylon shape. In this section, the nacelle position and shape, and wing shape are frozen to the previous optimal geometry (*OPT1* configuration), and only the pylon is designed to be improved.

4.2 Problem Definition

4.2.1 Objectives and constraint

The objective functions and constraints are the same as previous section as shown below:

Objectives:
1. Maximise Cruise L/D
2. Minimise Nacelle Height (Z/c)
3. Minimise Nacelle Rearward Location (X/c)

Constraints:
1. constant C_L =0.57

Number of design variables: 15

Only the number of design variables is changed because pylon shape is modified in this optimisation.

4.2.2 Geometry Definition

The wing thickness of the pylon is defined by Bezier curve of four control points shown in Fig. 10 (a). There are seven design variables to control the wing thickness of the pylon. By using this geometrical definition, symmetrical airfoil of the pylon is represented. In addition, the camber is defined by Bezier curve of five control points shown in Fig. 10 (b). The camber is controlled by the x, y coordinates of four control points, which correspond to eight design variables. Finally, a new pylon shape is generated by combining the wing thickness of the pylon with the camber. Therefore, 15 design variables are used in total.

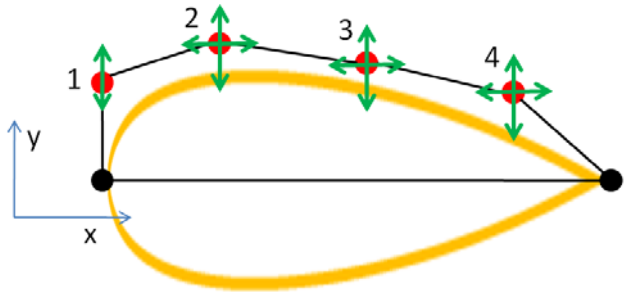

(a) Thickness Distribution

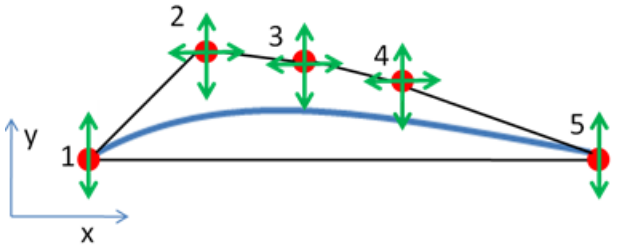

(b) Camber Distribution

Fig. 10 Pylon Shape Definition

4.3 Optimisation Results

The first Kriging model was constructed using 41 sample points of the Latin Hypercube sampling and the final Kriging model was constructed with 79 sample points in total after five updates.

The optimal design *OPT2* was obtained after the optimisation and L/D of 35.4 was achieved at the angle of attack of 5.85 degrees. The results of *OPT1* and *OPT2* geometries are described in Table 1. The difference of L/D is tiny but *OPT2* actually achieved 5 counts drag reduction compared to *OPT1*. The modified pylon shapes are plotted in Fig. 11. While the original SC(2)-0008 is symmetry, designed pylon has camber and different leading edge radius, where positive y/c is inboard wing side and negative y/c is outboard wing side. In Fig. 12, Mach contours of *OPT1* and *OPT1* are shown. According to the result, the *OPT2* reduces inboard shock waves due to the sharp leading edge and camber which enables to avoid flow acceleration between a wing and a nacelle. Pressure coefficient distributions at 32% and 37% semi-span location are also plotted in Fig. 13. This also indicates that inboard shock wave is weakened due to the pylon shape modification.

The pressure drag of the *OPT1* and the *OPT2* is shown in Fig. 14. It indicates that optimisation of the pylon shape is contributed to reduce the drag of inboard wing. On the other hand, the thrust of pylon is slightly weaker because the shock wave near the leading edge of pylon is reduced by the pylon shape optimisation.

Table 1 Pylon Thickness and L/D

	OPT1	*OPT2*
Pylon thickness	8.0%	9.0%
L/D	34.5	35.5

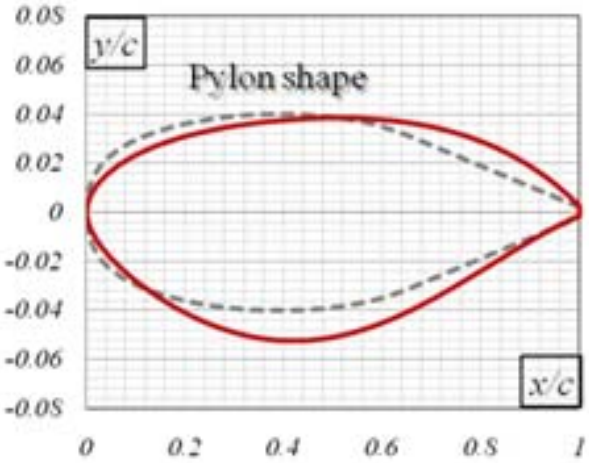

Fig. 11 Comparison of Pylon Shape
(blue: SC(2)-0008, red: *OPT2*)

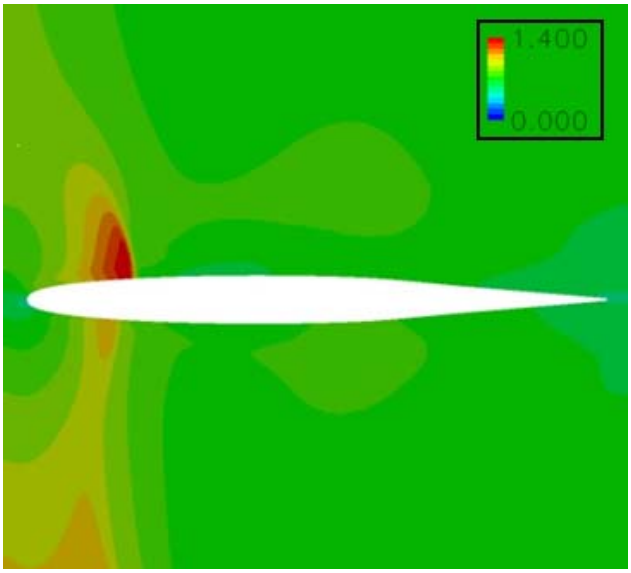

(a) *OPT1* Pylon (SC(2)-0008)

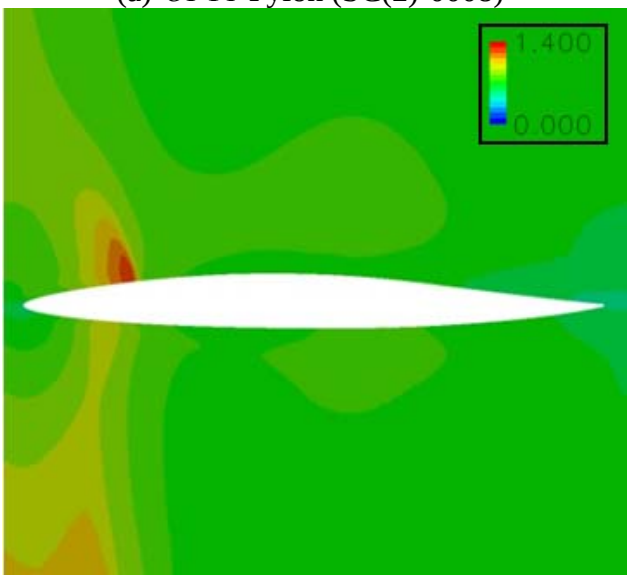

(b) *OPT2* Pylon (SC(2)-0008)

Fig. 12 Comparison of Mach Contours

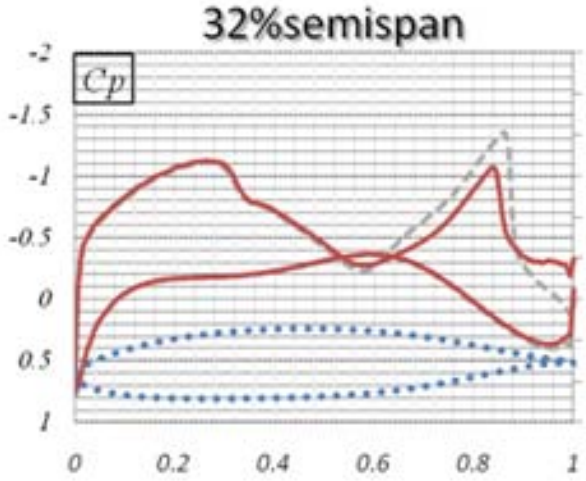

(a) 32% Semi-span Location

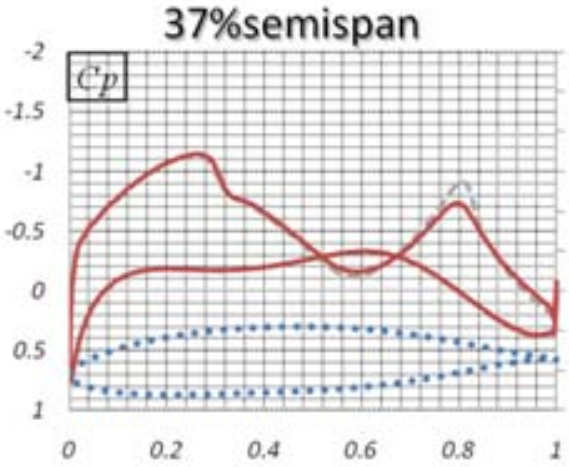

(b) 37% Semi-span Location

Fig. 13 Comparison of Cp Distribution
(black line: *OPT1*, red line: *OPT2*)

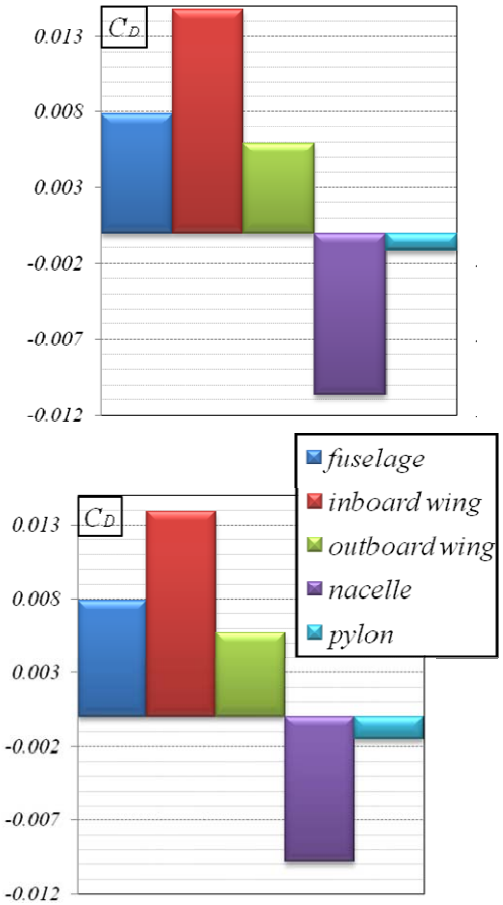

Fig. 14 Proportion of Pressure Drag Coefficient (above: *OPT1*, below: *OPT2*)

5 Performance of OWN Configuration

The feasibility of OWN configuration is discussed herein through the comparison with DLR-F6 configuration that is conventional UWN configuration. The original design Mach number of DLR-F6 is 0.75. However, the Mach number in this research is set to 0.70 to focus on a mid-sized, short-range aircraft. Though it is not fully fair comparisons, the cruise performances of DLR-F6 and optimised OWN based on *OPT2* at Mach number of 0.70 are compared in this section to investigate the aerodynamic feasibility of OWN configuration.

Surface pressure coefficient contours of both DLR-F6 and OWN configurations are shown in Fig. 15. The aerodynamic performances are summarised in Table 2, and pressure drag components are plotted in Fig. 16. From this result, it demonstrates that optimised OWN configuration is able to achieve higher L/D than that of DLR-F6 configuration. This proves that OWN configuration has a potential to achieve high L/D comparable to conventional UWN by applying optimisation techniques. When OWN configuration is realised, it is expected that the length of a landing gear can be much shortened compared to that of UWN configuration. This enables to reduce the total weight of the aircraft, which also leads the increase of aerodynamic performance. In addition, as mentioned above, OWN configuration has an advantage of a shielding effect of the noise propagation toward the ground caused by fan and jet noises. By conducting further optimisation integrating all the components at various flight conditions, OWN configuration will be able to prove that it is a potential candidate to be a near-future aircraft.

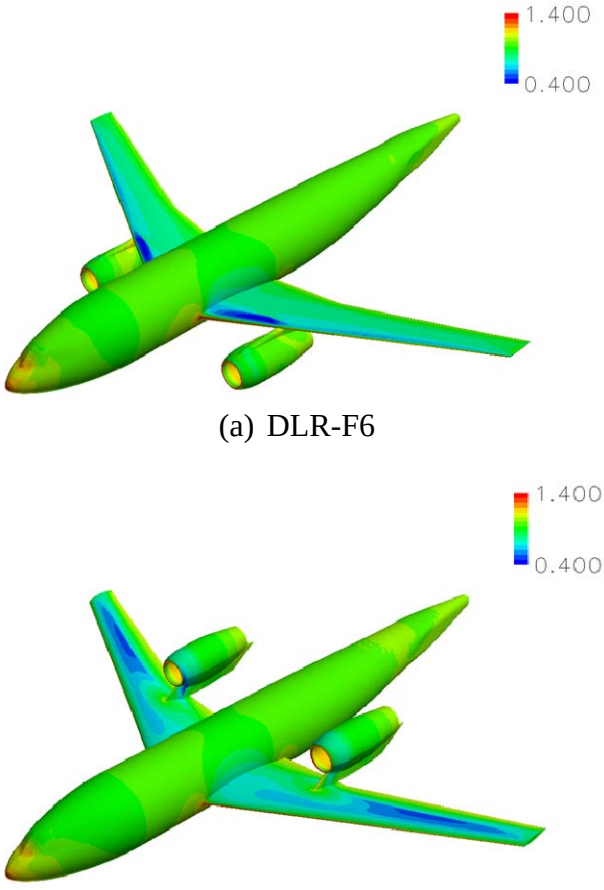

(a) DLR-F6

(b) OWN (*OPT2*) Geometry

Fig. 15 Comparison of Surface Pressure Coefficient Contours

Table 2 Cruise Performance of DLR-F6 and OWN (*OPT2*) Configurations

	DLR-F6	OWN (*OPT2*)
L/D	31.7	35.5

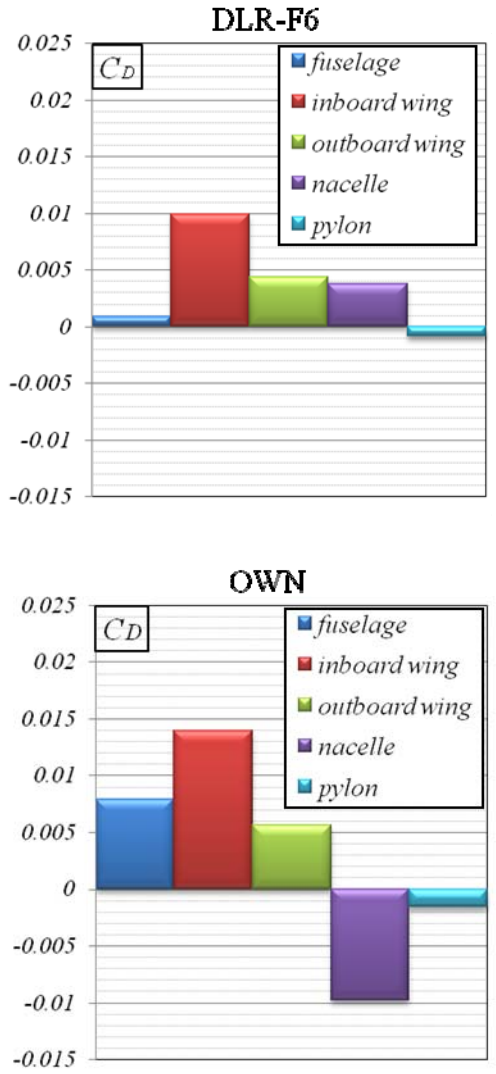

Fig. 16 Proportion of Pressure Drag Coefficient (above: DLR-F6, below: OWN-*OPT2*)

6 Conclusions

Aerodynamic optimisations of OWN configuration were conducted by modifying nacelle position, nacelle shape, wing shape and pylon shape to investigate the usefulness of an OWN configuration. Firstly, the nacelle position and its shape as well as wing shape were optimised to maximise L/D and to achieve preferable nacelle position for a realistic aircraft design in terms of structural and maintenance points of view. As a result of the optimisation, optimal configuration (*OPT1*) achieved L/D of 34.5. It reveals that the nacelle position is highly related to aerodynamic performance of OWN configuration, however, reasonable L/D can be obtained by the modification of nacelle and wing shape even when the nacelle is close to a wing.

Secondly, the pylon shape of the above optimal configuration was further optimised to reduce the interference effect between a wing and a nacelle. As a result of the optimisation, the buffet near the trailing edge was weakened compared with original pylon shape. This enabled to achieve higher L/D of 35.5 corresponding to 5 drag counts reduction from the first optimisation. The optimal geometry (*OPT2*) is compared with DLR-F6 as a representative of conventional UWN. It proves that cruise performance of OWN can be comparable to that of UWN. Through the present aerodynamic optimisations of OWN configuration, it is concluded that an aerodynamically-efficient OWN configuration comparable to conventional UWN will be realised feasible with further optimisation under the various flight conditions and further integrated optimisation of nacelle, wing, pylon and fuselage configuration.

7 Contact Author Email Address

sasaki@ad.mech.tohoku.ac.jp

Acknowledgements

The present computation was executed by using NEC Vector Supercomputer of SX-9 in Cyberscience Center of Tohoku University.

References

[1] Ricouard J, Davy R, Loheac P, Moore A and Piccin O. ROSAS Wind Tunnel Test Campaign Dedicated to Unconventional Aircraft Concepts Study. AIAA Paper 2004-2867, 10th AIAA/CEAS Aeroacoustics Conference, Manchester, UK, May 10-12, 2004.

[2] Nakahashi K, Ito Y and Togashi F. Some Challenges of Realistic Flow Simulations by Unstructured Grid CFD. *International Journal for Numerical Methods in Fluids*, Vol. 43, pp 769-783, 2003

[3] Sunago M, Sasaki D, Takenaka K and Nakahashi K. Multipoint Optimization of a Short-Range Quiet Passenger Aircraft. *Journal of Aircraft*, Vol. 46, No. 3, pp 1070-1074, May-June 2009.

[4] Obayashi, S and Guruswamy G P. Convergence Acceleration of a Navier-Stokes Solver for Efficient Static Aeroelastic Computations. *AIAA Journal*, Vol. 33, No. 6, pp 1134-1141, 1995.

[5] Venkatakrishnan V. On the Accuracy of Limiters and Convergence to Steady State Solutions. AIAA Paper 93-0880, 1992.

[6] Sharov D and Nakahashi K. Reordering of Hybrid Unstructured Grids for Lower-Upper Symmetric Gauss-Seidel Computations. *AIAA Journal*, Vol. 36, No. 3, pp 484-486, 1998.

[7] Sasaki D and Obayashi S. Efficient Search for Trade-Offs by Adaptive Range Multi-objective Genetic Algorithms. *Journal of Aerospace Computing Information, and Communication*, Vol. 2, No. 1, pp 44-64, 2005.

[8] Jeong S, Minemura Y and Obayashi S. Optimization of Combustion Chamber for Diesel Engine Using Kriging Model. *Journal of Fluid Science and Technology*, Vol. 1, pp 138-146, 2006.

[9] Jeong S, Murayama M and Yamamoto K. Efficient Optimization Design Method Using Kriging Model. *Journal of Aircraft*, Vol. 42, pp 413–420, 2005.

[10] Mckay M D, Beckman R J and Conover W J. A Comparison of Three Methods for Selecting Values of Input Variables in the Analysis of Output from a Computer Code. *Technometrics*, Vol. 21, No. 2, pp 239-245, 1979.

[11] Data available on line at http://aaac.larc.nasa.gov/tsab/cfdlarc/aiaa-dpw/Workshop3/DPW3-geom.html

[12] Sobieczky H. Parametric Airfoils and Wings. *Notes on Numerical Fluid Mechanics*, pp 71-88, 1998.

[13] Ito Y and Nakahashi K. Surface Triangulation for Polygonal Models Based on CAD Data. *International Journal for Numerical Methods in Fluids*, Vol. 39, No. 1, pp 75-96, 2002.

[14] Sharov D and Nakahashi K. Hybrid Prismatic/Tetrahedral Grid Generation for Viscous Flow Applications. *AIAA Journal*, Vol. 36, No. 2, pp 157-162, 1998.

Copyright Statement